Polyisoprene–Polystyrene Diblock Copolymer Phase Diagram near the Order–Disorder Transition

Ashish K. Khandpur,[†] Stephan Förster,[‡] and Frank S. Bates*

Department of Chemical Engineering & Materials Science, University of Minnesota, Minneapolis, Minnesota 55455

Ian W. Hamley

Science Laboratories, Department of Physics, University of Durham, South Road, Durham DH1 3LE, U.K.

Anthony J. Ryan

Materials Science Center, UMIST, Grosvenor Street, Manchester M1 7HS, U.K., and CLRC Daresbury Laboratory, Warrington WA4 4AD, U.K.

Wim Bras[§]

CLRC Daresbury Laboratory, Warrington WA4 4AD, U.K.

Kristoffer Almdal and Kell Mortensen

Risø National Laboratory, DK-4000 Roskilde, Denmark

Received May 30, 1995; Revised Manuscript Received September 14, 1995[⊗]

ABSTRACT: The phase behavior of ten polyisoprene–polystyrene (PI–PS) diblock copolymers, spanning the composition range from 0.24 to 0.82 polyisoprene volume fraction (f_{PI}), has been studied near the order–disorder transition (ODT). Dynamic mechanical spectroscopy, transmission electron microscopy, and neutron and X-ray scattering have been used to characterize phase transition temperatures and ordered state symmetries. Five distinct microstructures were observed for this chemical system: spheres, hexagonally packed cylinders (HEX), lamellae (LAM), hexagonally perforated layers (HPL), and a bicontinuous cubic phase having an $Ia\bar{3}d$ space group symmetry. The bicontinuous $Ia\bar{3}d$ phase only occurs in the vicinity of the ODT between the HEX and LAM states at compositions of $0.65 \lesssim f_{PI} \lesssim 0.68$ and $0.36 \lesssim f_{PI} \lesssim 0.39$ (prior report). Farther from the ODT, within these composition ranges, the HPL phase occurs. We did not find the ordered bicontinuous double diamond (OBDD) morphology at any composition or temperature studied, and the overall phase diagram is qualitatively different from those reported previously for PI–PS block copolymers.

1. Introduction

Block copolymers are a type of amphiphile that can self-assemble into a variety of ordered microstructures. The associated bulk state phase behavior is strikingly similar to that exhibited by certain liquid crystalline materials, although a formal connection to these low molecular weight systems has yet to be established, either theoretically or experimentally. On one hand, thermotropism is plainly evident; the familiar lamellar phase in diblock copolymers is properly defined as an $\tilde{S}_{A2}$ smectic,[1] which disorders upon heating. In fact, a host of thermally induced order–order phase transitions have now been demonstrated in block copolymer melts. On the other hand, all of the morphologies found in block copolymers are also observed in lyotropic liquid crystals that contain two or more components; BCC spheres ($Im\bar{3}m$ space group), hexagonally packed cylinders (HEX), lamellae (LAM), and the recently identified $Ia\bar{3}d$ bicontinuous (also denoted "Gyroid*") phases have been known to the field of lipids and surfactants for nearly three decades.[2,3] This suggests that varying the composition, f, in block copolymers is analogous to changing the water content in the lyotropic systems. (An even closer correspondence exists for homopolymer/block copolymer mixtures.) In recent years, we have been exploring these connections in an effort to uncover the universal parameters that control order and disorder in block copolymer melts. Within mean-field theory, two parameters, χN and f, dictate block copolymer phase behavior, where χ is the Flory–Huggins segment–segment interaction parameter and N is the degree of polymerization. Fluctuation effects introduce a third parameter $\bar{N} = a^6 v^{-2} N$, where $a = R_g(N/6)^{-1/2}$, in which R_g is the Gaussian coil radius of gyration and v is the segment volume. Conformational asymmetry[4] leads to a fourth parameter $\epsilon = \beta_1^2/\beta_2^2$, where $\beta^2 = a^2/6v$. Although $\bar{N}$ and ϵ can account for certain qualitative features in the experimental phase diagrams, there are still significant inconsistencies between theory and experiment. Failure of the theories[5–8] is likely to be most pronounced as $\bar{N}$ is decreased toward the liquid crystal limit. This paper describes our collective results for the lowest molecular weight block copolymer system that we have studied near the ODT to date.

Polyisoprene–polystyrene (PI–PS) and polybutadiene–polystyrene (PB–PS) block copolymers have been the subject of the majority of experimental studies[9–21] on block copolymer phase behavior. Most experiments have been conducted in the strong segregation limit (SSL) where the following morphologies are reported

* To whom correspondence should be addressed.
[†] Present address: 3M Co. Building 201-3E-03, St. Paul, MN 55144.
[‡] Present address: MPI-KGF, Kantstrasse 55, 14513 Teltow-Seehof, Germany.
[§] Present address: AMOLF, Kruislaan, Amsterdam, The Netherlands.
[⊗] Abstract published in *Advance ACS Abstracts,* November 15, 1995.

0024-9297/95/2228-8796$09.00/0

upon increasing the volume fraction of polyisoprene, f_{PI}: [12] BCC–HEX–OBDD–LAM–OBDD–HEX–BCC. Here OBDD stands for an ordered bicontinuous double diamond structure ($Pn\bar{3}m$ space group). The OBDD structure was first identified by Thomas et al.[13] in star block copolymers and subsequently reported in a variety of block copolymers[14–16] and block copolymer–homopolymer mixtures.[17,18] Since the LAM, HEX, and BCC morphologies have been well documented and the composition dependence of these microstructures is in good agreement with theoretical calculations in the SSL,[6] we shall refer to them as "classical" phases. Theoretical attempts have failed to explain the occurrence of the OBDD phase, and calculations find this phase to be, at best, metastable.[22–25] Recently, two nonclassical morphologies, hexagonally perforated layers (HPL) and a bicontinuous cubic phase bearing an $Ia\bar{3}d$ space group symmetry, were identified by us in certain $f_{PI} < 0.5$ PI–PS diblock copolymers.[26] Hajduk et al.[27] have also reported the $Ia\bar{3}d$ bicontinuous (or "Gyroid*") phase in an $f_{PI} = 0.67$ diblock specimen. We also reported that at equilibrium the bicontinuous $Ia\bar{3}d$ phase appears only within 60 °C of the order–disorder transition (ODT), although it displays a remarkable metastability when cooled below the HEX ↔ $Ia\bar{3}d$ or HPL ↔ $Ia\bar{3}d$ order–order transition temperatures. Long-time annealing and/or shearing was required to obtain the low-temperature equilibrium microstructures. These findings complement other work in our group with model polyolefin and polystyrene–poly(2-vinylpyridine) diblock copolymers, where the HPL and bicontinuous $Ia\bar{3}d$ phases have also been observed.[28–30] However, the occurrence of these complex phases appears to be nonuniversal in the classical parameters χN and f. In fact, for the highest molecular weight system examined (i.e., largest $\bar{N}$), the bicontinuous cubic phase is completely absent.[31] Taken together, our results indicate that $\bar{N}$ plays a central role in the occurrence of the complex phases; for symmetric ($f = 1/2$) PE–PEP, PEP–PEE, PE–PEE, and PS–PVP, a value of $\bar{N} = 2.7 \times 10^3$, 3.4×10^3, 3.3×10^3, and 1.1×10^3, respectively, places the ODT at 150 °C.[31] We have turned to PI–PS since it is composed of relatively incompatible blocks, and accordingly a rather small value of $\bar{N}$ is dictated when the ODT occurs at experimentally tractable temperatures; $\bar{N} \cong 1.1 \times 10^3$ when $T_{ODT} = 150$ °C for $f = 1/2$.

In the present study, we report the phase behavior of PI–PS diblock copolymers near the ODT for polyisoprene volume fractions $0.24 \lesssim f_{PI} \lesssim 0.82$. Based on our previous work with $f_{PI} < 0.5$ specimens,[26] we anticipated a rich phase behavior near the ODT, at compositions around the LAM ↔ HEX transition for $f_{PI} > 0.5$. It is in this composition window that the intriguing OBDD phase has been reported for both diblock[14] and star-block[13] copolymers. To date, our work on PI–PS diblock copolymers and a number of other chemical systems has failed to reveal the OBDD morphology. Here we expand on the effort begun earlier[26] and report a comprehensive phase diagram for PI–PS diblocks near the ODT based on our results. (A comprehensive comparison with all other studies of PI–PS phase behavior, which goes beyond the scope of this paper, will be presented in a future report.) Nearly monodisperse specimens were prepared by anionic polymerization; a total of 16 low molecular weight PI–PS samples have now been studied near their ODT by us. Phase transitions have been established by dynamic mechanical spectroscopy and phase symmetry by transmission electron microscopy (TEM) and small-angle X-ray (SAXS) and neutron (SANS) scattering. Based on these results, we conclude that the PI–PS phase diagram contains at least five different morphologies: spheres ($Im\bar{3}m$), cylinders (HEX), hexagonally perforated layers (HPL), bicontinuous ($Ia\bar{3}d$), and lamellae (LAM).

Table 1. Molecular Characteristics of PI–PS Diblock Copolymers

sample	f_{PI}	$10^{-4}M_n$	phase transitions[a,b]
IS-24[c]	0.24_2	5.44	C $\xrightarrow{293}$ E $\xrightarrow{309}$ Dis
IS-54[d]	0.54_0	1.70	A $\xrightarrow{124}$ Dis
IS-63	0.62_6	3.46	A $\xrightarrow{247}$ Dis
IS-64	0.64_2	3.98	A $\xrightarrow{267}$ Dis
IS-65	0.65_1	3.95	A $\xrightarrow{190}$ D $\xrightarrow{221}$ B $\xrightarrow{279}$ Dis
IS-66	0.66_4	3.97	A $\xrightarrow{159}$ D $\xrightarrow{210}$ B $\xrightarrow{268}$ Dis
IS-68	0.67_5	3.99	A $\xrightarrow{134}$ D $\xrightarrow{198}$ B $\xrightarrow{252}$ C $\xrightarrow{267}$ Dis
IS-69	0.69_2	3.98	B $\xrightarrow{166}$ C $\xrightarrow{265}$ Dis
IS-70	0.70_4	3.47	C $\xrightarrow{177}$ Dis
IS-82	0.82_0	7.91	C $\xrightarrow{300}$ Dis

[a] Numbers above arrows indicate the phase transition temperatures in °C as determined from dynamic mechanical measurements. [b] Phase allocations are as follows: A, lamellae; B, bicontinuous cubic ($Ia\bar{3}d$); C, hexagonally packed cylinders; D, hexagonally perforated layers; E, BCC spheres ($Im\bar{3}m$). [c] The high-temperature E phase in IS-24 is identified as BCC spheres based on the rheological signature. [d] Reported in ref 53.

This paper is organiized as follows. In section 2 we present the experimental techniques and procedures applied to study the PI–PS diblock copolymer phase behavior. This is followed in section 3 by an analysis of the dynamic mechanical spectroscopy, TEM, SANS, and SAXS results. In section 4 we discuss our findings in the context of an overall phase diagram for the PI–PS system close to the ODT and comment on the important of fluctuation effects and on the reversibility of the different phase transitions observed. We summarize our findings in section 5.

2. Experimental Section

2.1. Synthesis and Sample Preparation. PI–PS diblock copolymers were synthesized by anionic polymerization using established procedures.[32] The polymerization was carried out at 40 °C using *sec*-butyllithium as the initiator and cyclohexane as the solvent. These conditions lead to attactic polystyrene and a high degree of 1,4-addition of isoprene (75% cis-1,4; 20% trans-1,4; 5% 3,4 addition).[33] The compositions of the diblock copolymers were calculated from the masses of the added monomers; the yield was greater than 99% in all cases. The volume fraction of polyisoprene, f_{PI}, was estimated using the densities 1.05 and 0.90 g/cm^3 for PS and PI, respectively. The compositions and molecular weights of 10 samples are given in Table 1. M_n has been calculated from the monomer/initiator ratio, which, from our experience, provides the most quantitative measure of M_n. A measure of our success in targeting M_n is provided by the consistent placement of the ODT temperature (see below) within a desired range. All of the synthesized diblock copolymers had a relatively narrow polydispersity ($M_w/M_n < 1.07$), which was determined by size exclusion chromatography (SEC). This method also provided a relative measure of the overall molecular weight and confirmed the absence of homopolymer.

Most of the experimental data presented here were obtained on pristine specimens that did not contain antioxidant. Since thermal degradation is a concern when dealing with unsaturated polymers, we also conducted a number of control experiments with samples containing 0.2 wt % BHT, an antioxidant. Dynamic mechanical spectroscopy and transmission electron

microscopy (TEM) results did not reveal noticeable differences between the samples that did and did not contain BHT. For example, the IS-68 sample, which shows the maximum number of ordered microstructures (four; see below), yielded virtually identified results when prepared with or without BHT. Previous work[26] with PI−PS polymers also demonstrated that our experimental procedures do not lead to significant amounts of degradation or variability in phase behavior. Therefore, we presently report all our results without discriminating between samples that contain and do not contain BHT.

Rheology and small-angle neutron scattering (SANS) specimens were prepared as 0.3−2 mm thick films in the following way. The polymer, together with a spacer of required film thickness, was placed between two Teflon-covered glass plates and heated to 120 °C for about 15 h under vacuum. The weight of the plate caused the polymer to deform into a transparent film, which was then cooled to room temperature while still under vacuum.

For TEM and small-angle X-ray scattering (SAXS), the polymer was sealed in evacuated ($<10^{-2}$ Torr) ampules and annealed at the desired temperature for 2−20 h. The annealing time was decreased with the annealing temperature in order to minimize the possibility of thermal degradation. Annealing was accomplished by immersing the ampule in a temperature-controlled oil bath, after which the ampule was quenched in liquid nitrogen. This froze the microstructure present at the annealing temperature since PS forms a glass at or below about 100 °C. (The PS glass transition temperature will be suppressed by as much as 10 °C due to the low block molecular weights.[34]) In all cases, prior to the final annealing step, we heated the polymer above T_{ODT} for 20 min to remove any effects induced by the prior thermal or processing history and then quenched the specimen in liquid nitrogen. This was followed by annealing in the temperature window corresponding to the lowest temperature ordered phase as identified rheologically. Subsequently, the final annealing step was performed.

2.2. Dynamic Mechanical Experiments. Dynamic mechanical spectroscopy (DMS) experiments were conducted on a Rheometrics RSA II solids analyzer operated in the oscillatory mode using a shear sandwich fixture at a shear amplitude of 5%. In this work, we report isochronal (ω = 0.1 or 1 rad/s) measurements of the dynamic elastic modulus, G', obtained as the temperature was increased at 1 or 2 °C/min. In a series of papers, we have shown that $G'(T)$ provides a convenient fingerprint of the phase behavior in block copolymer melts. Abrupt changes in G' can be associated with order−order and order−disorder transitions.[26,28,29,30,35] Here we note that the results of the dynamic mechanical measurements can be affected by the choice of experimental parameters. Recent experiments with lamellar-forming PI−PS diblocks[36] and bicontinuous PE−PEE specimens[37] indicate that nonlinearity in the mechanical response becomes evident at strain amplitudes above roughly 1%. This leads to a frequency-dependent reduction in G' and G'' due to microdomain alignment (e.g., in lamellar samples) or defect generation (e.g., in cubic samples[38]). However, we are presently primarily interested in identifying abrupt changes in G' for the purpose of establishing phase transition temperatures, and these do not appear to be influenced by strain amplitude at the modest level employed here.

2.3. Transmission Electron Microscopy. A Reichert Ultracut S microtome was used to obtain ultrathin sections (50−70 nm) for transmission electron microscopy (TEM). Sections were cut at −100 °C using a diamond knife. These were collected (dry) on 400 mesh uncoated copper grids and then strained in the vapor of a 1.5% aqueous osmium tetraoxide (OsO_4) solution for 5−10 h. Since the PI microphase is preferentially stained by OsO_4, it appears dark under bright-field TEM. TEM was conducted in the bright-field mode on JEOL 100CX and JEOL 1210 electron microscopes operated at 100 and 120 kV accelerating voltages, respectively.

2.4. Small-Angle X-ray Scattering. SAXS measurements were performed at the CLRC synchrotron facility at Daresbury, Warrington, England. The X-ray beam was monochromated with Ge(111) crystals to a wavelength $\lambda = 1.50 \pm 0.01$ Å. The scattered radiation was recorded on a quadrant area detector that extends radially 0.2 m and covers an opening area of 70° with a spatial resolution of 500 μm. A detailed description of this facility can be found elsewhere.[39] The results presented here were obtained from polycrystalline (i.e., polydomain) specimens in a powdered form at room temperature for most cases. Since PS is glassy below about 100 °C, the established morphology at elevated temperatures could be arrested by rapidly cooling below the glass transition temperature of PS. TEM and SAXS were conducted on different pieces of the same sample in order to best correlate the real and reciprocal space experiments. For sample IS-68, SAXS was also conducted at temperatures above the glass transition in different ordered states. For such experiments, the sample (~0.75 mm thick) was placed in a differential scanning calorimetry (DSC) pan with mica windows. The pan was held on a Linkam microscope hotstage under a flow of nitrogen and its temperature monitored with a thermocouple that was taped to it. Scattering patterns were averaged azimuthally to give the one-dimensional form of intensity (arbitrary units) as a function of the scattering wavevector, $|\mathbf{q}| = q = 4\pi\lambda^{-1}\sin(\theta/2)$, where θ is the scattering angle.

2.5. Small-Angle Neutron Scattering. SANS measurements were performed at the Risϕ National Laboratory using pinhole collimation, λ = 6.0 Å wavelength neutrons ($\Delta\lambda/\lambda$ = 0.09), and a 6 m sample-to-detector distance. An *in-situ* reciprocating shearing device provided for online shearing of the sample, which allowed us to align certain microstructures at a macroscopic scale. A more detailed discussion of the shearing device is presented elsewhere.[29,38] The specimen was held between temperature-controlled (within 1 °C) aluminum plates separated by a distance of 0.3 mm. The shearing device is operated under a helium atmosphere to prevent degradation. Scattering data were acquired on an area detector, and the intensities are reported in arbitrary units. Neutron scattering relied on the weak natural contrast between hydrogenous PS and PI.

3. Results and Analysis

3.1. Dynamic Mechanical Analysis. Rheology is a convenient and effective tool for identifying order−disorder (ODT) and order−order (OOT) phase transitions in block copolymer melts. Here we have used low-frequency isochronal G' measurements to guide the selection of temperatures for TEM and small-angle scattering experiments. Figure 1 contains measured G' traces for seven of the ten polymers listed in Table 1. Since the primary focus of this paper is the windows of complex phase behavior between the LAM and HEX states, we have omitted the f_{PI} = 0.24, 0.54, and 0.82 results. Order−order transitions are marked by open arrows, while order−disorder transitions are shown by filled arrows. Samples IS-63, IS-64, and IS-70 (Figure 1a,b,g, respectively) appear to exhibit a single ordered phase before disordering, while sample IS-69 exhibits two ordered microstructures (Figure 1f), and samples IS-65 and IS-66 show three ordered phases (Figure 1c,d). A maximum number of four ordered phases was observed in sample IS-68 (Figure 1e). The regions marked A, B, C, and D correspond to lamellar, bicontinuous, cylindrical, and perforated layered microstructures, respectively, as described below. As shown in earlier publications,[26,40] the isothermal frequency response of a diblock copolymer in a particular ordered state is quite distinctive and can provide a valuable clue as to the associated microstructure. We have chosen to omit these results here but note that they are nearly identical to those reported in our earlier PI−PS publication.[26] The OOT and ODT temperatures identified by the open and solid arrows, respectively, are listed in Table 1.

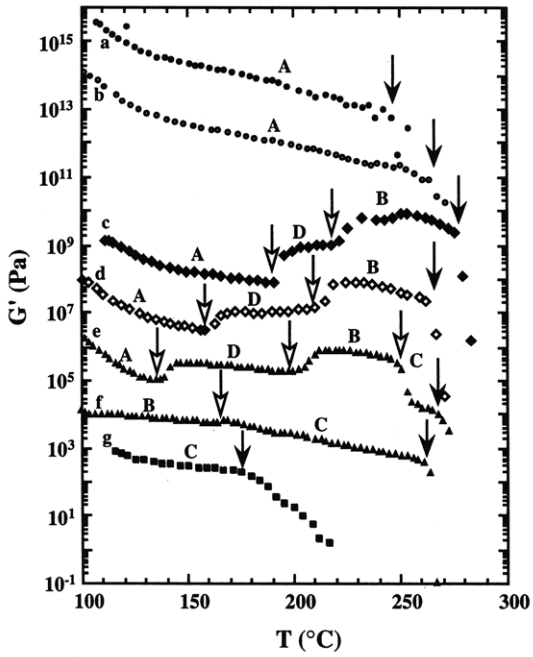

Figure 1. Dynamic storage modulus (G') as a function of temperature for (a) IS-63, (b) IS-64, (c) IS-65, (d) IS-66, (e) IS-68, (f) IS-69, and (g) IS-70. A frequency of 0.1 rad/s and a heating rate of 2 °C/min was used for all samples except IS-68 and IS-69, where these parameters were 1 rad/s and 1 °C/min, respectively. A strain amplitude of 5% was applied in all cases. Open and filled arrows indicate order–order and order–disorder phase transitions, respectively. The data have been multiplied by the following factors: (a) 10^{12}, (b) 10^{10}, (c) 10^{6}, (d) 10^{4}, (e) 10^{2}, (f) 10^{1}, (g) 10^{0}.

Since most of the disordering temperatures for our samples were relatively high (>200 °C), precautionary measures were taken to minimize thermal degradation during experimentation. Exposure to high temperatures (T > 200 °C) was limited to less than an hour in the dynamic mechanical spectrometer, which was operated using a nitrogen blanket. We also studied the effects of adding the antioxidant BHT in samples IS-64, IS-68, and IS-69. Dynamic mechanical data on these samples were virtually identical to those obtained from samples containing no BHT. A SEC trace obtained from a IS-24 specimen that was heated to 320 °C during an isochronal $G'(T)$ measurement, the highest temperature used in this work, displayed only minor degradation; less than 5% of the relatively monodisperse response obtained from the pristine material was transformed to lower or higher retention volumes.

Consistent with our earlier study,[26] we found that state B (bicontinuous $Ia\bar{3}d$; see below) persists upon cooling, all the way down to the PS glass transition temperature. This metastability can be eliminated by long annealing times (>10 h) and/or application of a shear field. However, B does not go back to phase C (cylinders) by annealing alone when C is the lower temperature equilibrium phase.[26] On heating, however, the B → C transformation is easily realized as shown by dynamic mechanical experiments (see Figure 1). Here we note that the change in G' associated with B → C is much less dramatic than that found when C → B.[26] We return to these differences in the behavior of the B ↔ C transition during heating and cooling in the discussion section.

3.2. Transmission Electron Microscopy. TEM was used to identify the microstructures associated with states A and C and to establish certain characteristic features of phases B and D. Representative micrographs of single-phase specimens containing lamellar (IS-64 annealed at 150 °C) and cylindrical (IS-82 annealed at 150 °C) microstructures are shown in Figure 2.

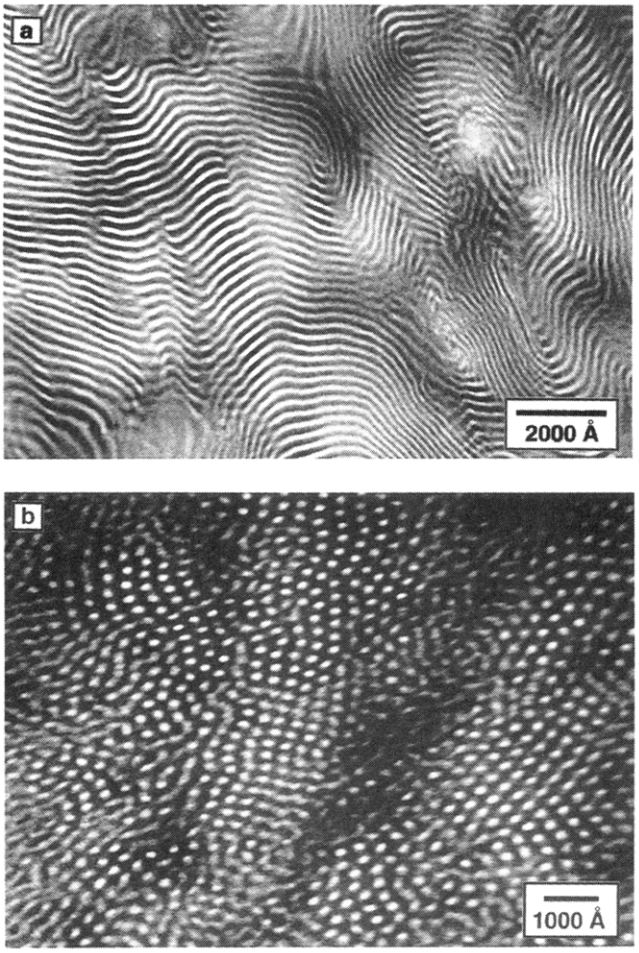

Figure 2. TEM micrographs from single-phase specimens: (a) IS-64; (b) IS-82. A lamellar microstructure is assigned to (a), while hexagonally packed cylinders of PS in a PI matrix are assigned to (b). Sample preparation consisted of annealing the specimens at 150 °C in vacuum for 10 h followed by a liquid nitrogen quench.

Since all four phases were observed in IS-68, we present micrographs obtained from this sample in Figures 3–6. Capturing these images was the most challenging of the TEM experiments, and these results are representative of the remaining TEM data obtained from each ordered region identified rheologically. Figure 3 shows the microstructure of phase A (annealed at 120 °C), which is clearly lamellar (LAM). Phase C was found to be hexagonally packed cylinders (HEX) of the minority PS block in a PI matrix as shown by Figure 4. Here we note that the apparent lack of long-ranged ordering in this image probably derives from the proximity of this phase to the ODT and from a relatively short annealing time at 260 °C. A typical image of state B (annealed at 220 °C) can be seen in Figure 5. This morphology appears to be bicontinuous with both three-fold (Figure 5) and four-fold (not shown) symmetry elements, suggesting an overall cubic symmetry. There is an obvious resemblance between these TEM micrographs and those associated with the OBDD phase. The "wagon wheel" morphology evident in Figure 5 looks identical to the reported [111] projection of the OBDD phase.[13,14] However, the SAXS and SANS data obtained

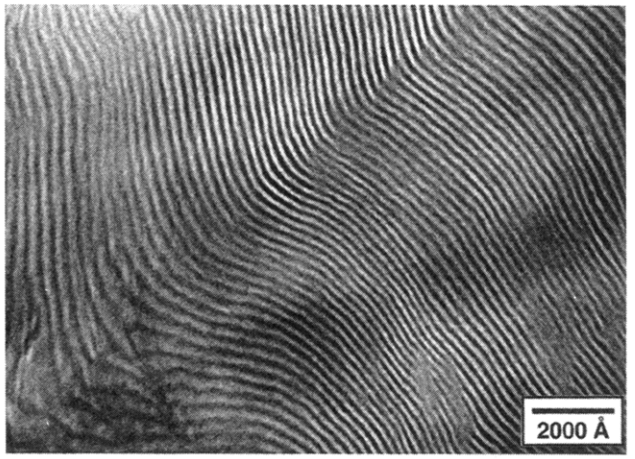

Figure 3. TEM micrograph from sample IS-68. The sample was annealed at 120 °C for about 5 h in vacuum and subsequently quenched in liquid nitrogen. A lamellar microstructure is assigned to phase A based on this and other similar results.

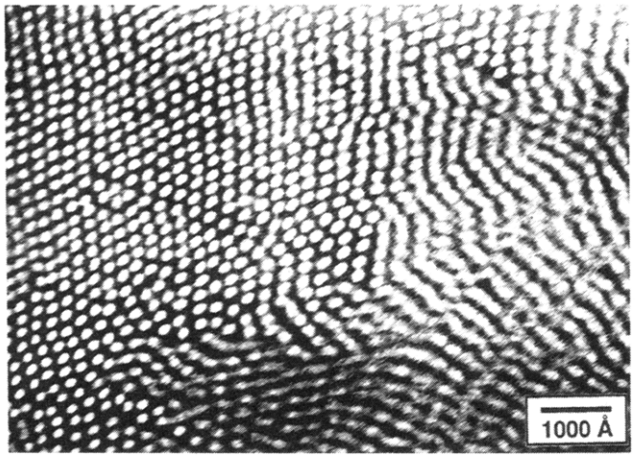

Figure 4. Representative TEM micrograph obtained from sample IS-68 after annealing at 260 °C for 2 h followed by quenching in liquid nitrogen. Hexagonally packed cylinders of polystyrene in a polyisoprene matrix have been associated to phase C based on this and other similar micrographs.

from state B are inconsistent with a $Pn\bar{3}m$ (OBDD) space group assignment as described below. Representative projections from state D (annealed at 145 °C) are shown in Figure 6. Alternating light (PS) and dark (PI) layers are seen with perforations in the minor component. The perforations seem to have a hexagonal symmetry (right inset), although this cannot be firmly established from TEM experiments alone. In another projection (left inset) a pseudohexagonal pattern of dark (PI) spots on a light (PS) background can be seen, which we interpret as a slice transverse to the layer plane. These views are consistent with the HPL phase, which has been reported before for other pure diblocks[26,40] as well as diblock/homopolymer mixtures.[17,41] Reversibility of the A → D and D → B transitions was demonstrated by cooling specimens of IS-68 from the D and B states and annealing for long times (>10 h). TEM analysis confirmed recovery of the adjacent lower temperature phase in each instance.

3.3. Small-Angle X-ray Scattering. TEM pictures of state B indicate a bicontinuous cubic microstructure. Neutron and X-ray scattering were utilized to assign a space group to this phase. SAXS was performed at room temperature on three samples (IS-66, IS-68, and IS-69) annealed and quenched in state B. For the sample IS-

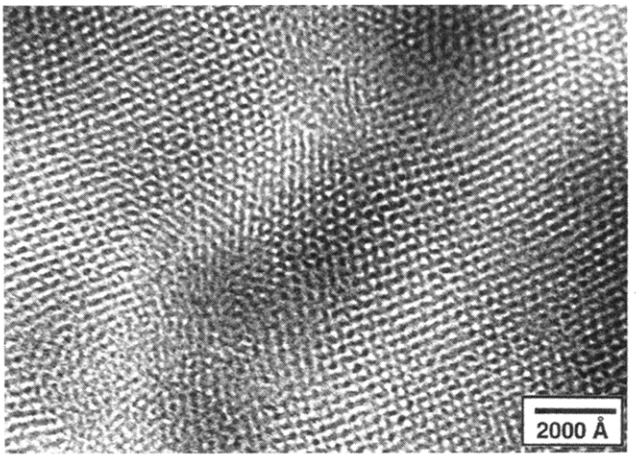

Figure 5. A commonly observed projection of the microstructure associated with phase B. Regions showing a "wagon wheel" type of morphology can be seen in this micrograph. The sample was IS-68, annealed at 220 °C for 3 h followed by a liquid nitrogen quench. Based on SAXS and SANS analysis, we have identified this as the bicontinuous $Ia\bar{3}d$ morphology.

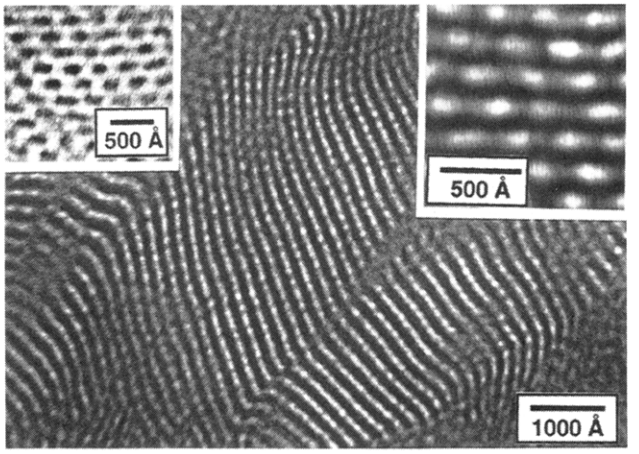

Figure 6. Representative projections of state D taken from sample IS-68 after annealing at 145 °C for 6 h followed by quenching in liquid nitrogen. Alternating light (PS) and dark (PI) layers are observed with perforations in the minor (PS) phase. The inset of the right provides a magnified view of this perpendicular orientation while the one on the left illustrates a section of the sample lying parallel on the microscope stage. In the latter, a hexagonal arrangement of PI perforations in the PS layer can be seen. Phase D is associated with the HPL morphology.

68, SAXS was also performed at temperatures corresponding to states B (240 °C) and D (150 °C).

Curves b and c of Figures 7 show the scattered intensity, I, versus normalized wave vector, q/q^*, for IS-68 at 240 °C and IS-66 at room temperature as a powder (quenched into liquid nitrogen after annealing at 220 °C), respectively. In both cases, the first two peaks have an intensity ratio of about 10:1 and occur at relative spacings of q^* and $1.15q^*$ as identified by the dashed lines. The overall scattering intensity of the molten specimen relative to the background level is lower than that for the quenched powder due primarily to the proximity of the former to T_{ODT}. Similar melt and quenched powder SAXS features were obtained from IS-66, IS-68, and IS-69 in state B. Consistency in the position and intensity of the first two SAXS peaks, the marked similarity of the TEM micrographs, similarity of the frequency response in the dynamical mechanical experiments, and the compositional proximity of samples IS-65, -66, -68, and -69 leads us to conclude that all four

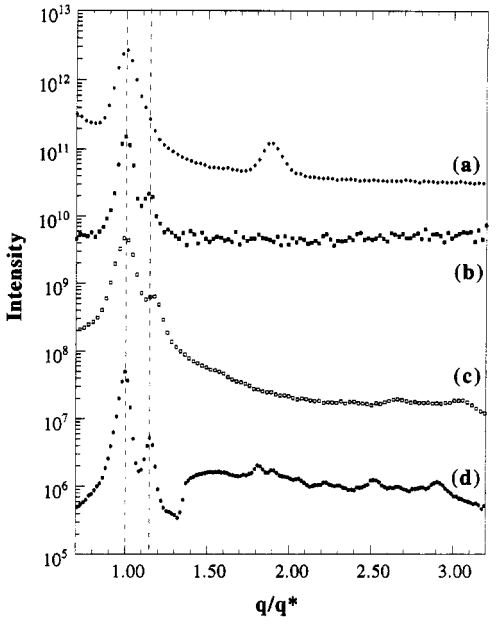

Figure 7. Small-angle X-ray scattering patterns obtained from PI–PS samples: (a) IS-68, T = 150 °C; (b) IS-68, T = 240 °C; (c) IS-66, room temperature powder (annealed at 220 °C for 3 h and then quenched in liquid nitrogen); (d) IS-39 room temperature powder (annealed at 200 °C for 3 h and then quenched; see ref 26). The low-q part of the detector was attenuated by a factor of 10 in trace d. The dashed lines identify q^* and $1.15q^*$.

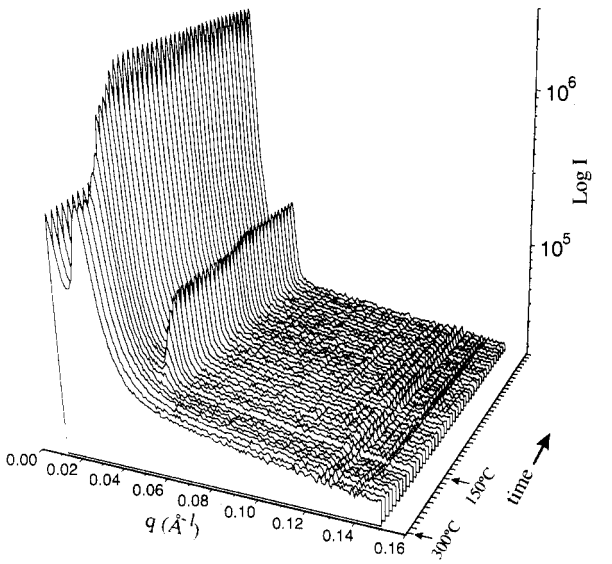

Figure 8. Growth of the HPL phase following a temperature quench from the disordered state. The sample (IS-68) was quenched from 300 to 150 °C and the scattered intensity monitored as a function of time. Each frame is separated by a time interval of 24 s. The quench was complete in about 5 min. The second-order peak develops at $1.88q^*$, where q^* is the position of the principal peak. This experiment shows that the HPL phase can be directly grown from the disordered state if the quench is fast enough. When the specimen is cooled slowly, the bicontinuous $Ia\bar{3}d$ phase develops and subsequently supercools to temperatures well below the HPL ↔ $Ia\bar{3}d$ transition.

polymers contain the same ordered microstructure in state B.

In Figure 7 we also compare the SAXS powder patterns obtained in this study from state B (Figure 7b,c) with one sample IS-39 (Figure 7d) previously[26] associated with the bicontinuous $Ia\bar{3}d$ state. The relative peak positions (q^*, $1.15q^*$) and intensities are essentially the same in each of these scattering patterns. However, the principal reflections from the IS-66 powder (Figure 7c) are noticeably broader than those from IS-39 (Figure 7d), and the former contains few identifiable higher order features; the IS-39 specimen produced at least 12 well-defined reflections (these are shown on a linear scale in ref 26). This general trend occurred consistently with all $f_{PI} > 0.5$ and $f_{PI} < 0.5$ room temperature powders that we have examined in state B. We speculate that these curious differences may derive from variations in the response to cooling below the glass transition temperature of polystyrene. The best SAXS data were obtained when the majority component was glassy at room temperature. Differential thermal contraction between PS and PI will create considerable stresses within the microstructure when the temperature is lowered below T_g for polystyrene, and perhaps a glassy minority domain succumbs to these thermal stresses. Nevertheless, the relative positions and intensities of the first two reflections are consistent with the bicontinuous $Ia\bar{3}d$ microstructure and inconsistent with OBDD; for the latter ($Pn\bar{3}m$ space group), the second reflection would occur at $1.22q^*$.

Figure 7a shows the SAXS pattern obtained from IS-68 at 150 °C, i.e., in state D. Unlike the 1:1.15 ratio of spacings for the first two peaks in state B, this ratio was found to be 1:1.88. TEM micrographs of state D indicate a layered-like morphology with in-plane perforations, which would be expected to result in first- and second-order reflections positioned at relative spacings of 1:2. At present, we do not have a conclusive explanation for the observed peaks at q^* and $1.88q^*$ for this microstructure. However, we have previously observed[40] this anomalous scattering behavior for the HPL phase in polyethylene–poly(ethylethylene) and poly(ethylene–propylene)–poly(ethylethylene) diblock copolymers, where the first two SANS reflections were observed at relative ratios between 1:1.75 and 1:2.

We also conducted time-resolved SAXS experiments of the growth of the HPL phase from the disordered state. Figure 8 shows the SAXS data for the IS-68 sample as it is rapidly cooled from 300 (disordered) to 150 °C. Each SAXS frame is separated by a 24 s time interval. It took about 5 min to cool from 300 to 150 °C under the experimental conditions employed. During this time, the scattering intensity continuously increased, indicating evolution of structure in the melt. In addition, a second-order peak developed at a relative spacing of about $1.88q^*$, which remained stable in position with further passage of time. This experiment shows that the higher temperature phases ($Ia\bar{3}d$ and HEX for this sample) can be bypassed, leading to the direct growth of the HPL phase if the specimen is cooled quickly enough from the disordered state. This result provides support for our conclusion, deduced from rheology measurements, that the HPL phase is at equilibrium at 150 °C in IS-68.

3.4. Small-Angle Neutron Scattering. SANS experiments were used to establish the in-plane packing symmetry of the perforations in phase D to corroborate the space group of phase B and to study the effect of shear rate on microstructure orientation in sample IS-68. For this purpose, an *in-situ* temperature-controlled shearing device[29,38] was employed. Shearing the sample allows us to induce long-range order, thereby elucidating certain symmetry elements not easily established with powders. Sample preparation consisted of reciprocating

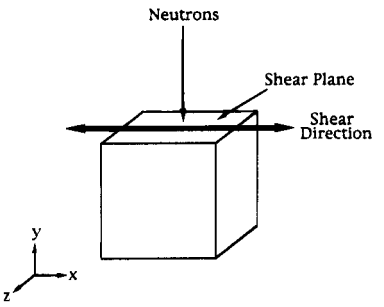

Figure 9. Deformation geometry and beam orientation for small-angle neutron scattering (SANS) experiments.

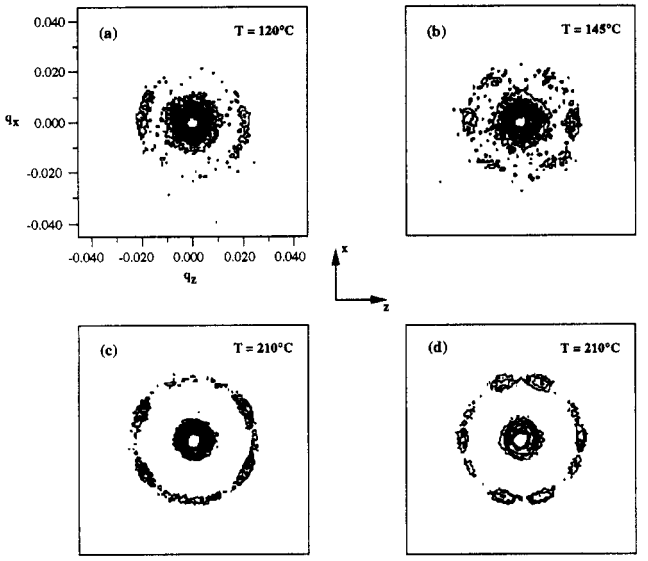

Figure 10. Contour plots of SANS patterns for the sample IS-68 in three different ordered states (A, D, B). A nearly featureless pattern (a) was observed in state A (120 °C), which is attributed to a parallel orientation of lamellae with respect to the shear plane. After heating the sample to 145 °C (state D) and application of dynamic shearing ($\dot{\gamma} = 0.1$ s^{-1} with $|\gamma| =$ 300%), a weak hexagonal scattering pattern was observed (b). This is consistent with a hexagonal in-plane arrangement of perforations in the minority (PS) layers. Further heating the sample to 210 °C, without shear (state B), produced a predominantly four-peak pattern (c), which transformed into result (d) when a shear rate of 2.2 s^{-1} was applied. The azimuthal relationship between the combined 10 reflections in (c) and (d) is consistent with the SANS data reported for sample IS-39 (ref 22) and the $Ia\bar{3}d$ space group symmetry.

shearing with a shear strain of $|\gamma| = 300\%$ on 0.3 mm thick specimens. Prior to making SANS measurements, the deformation field was stopped and the sample annealed for about 30 min. As discussed in several separate publications,[29,38,40] shearing block copolymers near the ODT can produce a complex, temperature-dependent and shear-rate-dependent response. In this work, we have simply exploited these behaviors in producing oriented lamellar, HPL, and $Ia\bar{3}d$ structures. A complete description of the dynamical properties of these microstructures is beyond the scope of this paper. However, the resulting broken symmetries are quite useful in further characterizing the equilibrium morphologies. Therefore, we presently identify each set of scattering patterns with a particular microstructure and orientation but make no effort to justify how they evolved. The deformation geometry and beam orientation are shown in Figure 9.

Figure 10a–d shows contour plots of scattered intensity on the q_x–q_z plane obtained from samples IS-68 at 120, 145, and 210 °C. These temperatures correspond to states A, D, and B, respectively, for this sample. Contour lines identify intensity on a linear scale, except for Figure 10d, which is based on a log scale. A weak, almost isotropic, scattering pattern is observed at 120 °C (Figure 10a). We believe, for reasons shortly discussed, that this corresponds to lamellae aligned parallel to the shear plane; this orientation can be attributed to the relatively low shear rate ($\dot{\gamma} = 0.1$ s^{-1}) applied to the sample.[42]

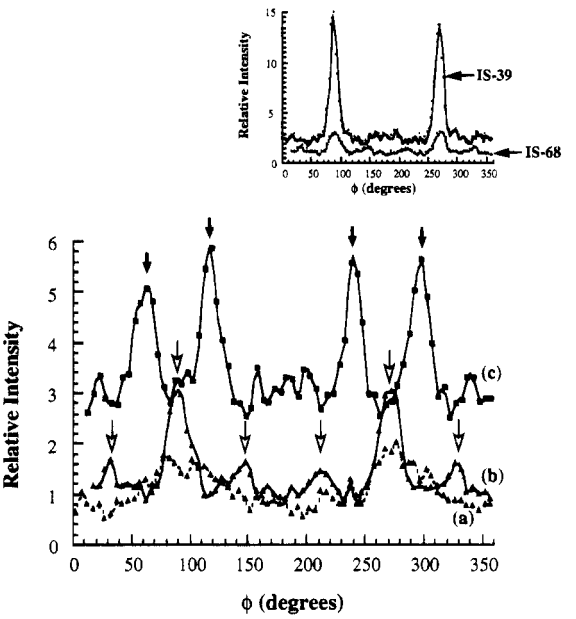

Figure 11. Azimuthal dependence of SANS intensities reported in Figure 10a–c. Data have been averaged over $\Delta q = q^* \pm 0.2q^*$ and are plotted as a function of ϕ, where $\phi = 0$ corresponds to $+x$. Open arrows identify increments of 60° (six-fold symmetry) while solid arrows are drawn at ±62 and ±118°. These peak positions are consistent with the HPL and $Ia\bar{3}d$ phase assignments, respectively. The inset compares the azimuthal intensity obtained from sample IS-39 with that from IS-68 (Figure 10b), both in the HPL phase. The former was shown earlier[26] to have a perpendicular orientation. The reduced intensity from IS-68 is consistent with a parallel alignment of perforated layers.

When the sample was heated to 145 °C and again sheared at a low shear rate ($\dot{\gamma} = 0.1$ s^{-1}) followed by quiescent annealing, the scattering pattern transformed into one with sixfold symmetry (Figure 10b); i.e., weak q^* reflections are observed at azimuthal angles of 60°. The peak positions are more clearly resolved when the scattered intensity is plotted as a function of azimuthal angle (ϕ) averaged over the band $\Delta q = q^* \pm 0.2q^*$ (i.e., centered on the peak wave vector q^*) as illustrated in Figure 11b. This indicates a hexagonal symmetry for the perforations identified by TEM (see Figure 6) and establishes the HPL microstructure for this phase. In a previous publication, we reported SANS patterns from another PI–PS specimens, IS-39 ($f_{PI} = 0.393$), that had been sheared while in a perforated layered state, leading to a "perpendicular" orientation where layer normals are directed perpendicular to the beam direction. The associated azimuthal $I(q^*)$ plot is also presented in the inset of Figure 11, for comparison with the present data for IS-68. Both data sets were acquired using identical conditions during the same experimental session, providing for a quantitative comparison. Clearly, the principal (equatorial) reflections from IS-39 are considerably more intense than those from IS-68, consistent with "perpendicular" and "parallel" layer alignment, respectively.

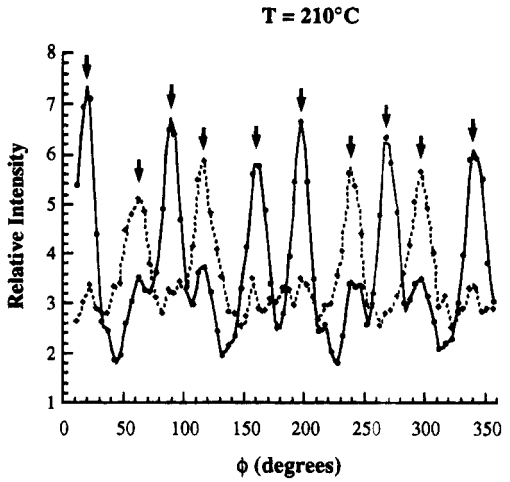

Figure 12. SANS intensity as a function of azimuthal angle, ϕ, for sample IS-68 at 210 °C. Data identified by the broken curve were reduced from Figure 10c, while those associated with the solid curve correspond to Figure 10d. The ten arrows identify the angular dependence expected for the epitaxial growth of the bicontinuous $Ia\bar{3}d$ phase from a shear-aligned lower symmetry phase.[26]

Heating the sample IS-68 to 210 °C converted the hexagonal SANS pattern found at 145 °C to a predominantly four-peak one, where the peaks are positioned at approximately $\phi = \pm 62$ and $\pm 118°$ with respect to the shear (i.e., x) axis (see Figures 10c and 11c). This is accompanied by an increase in the overall scattering intensity. These features are consistent with the HPL structure (with layer normals parallel to the incident neutron beam) transforming into the $Ia\bar{3}d$ state (a 3D network), guided by an epitaxial relationship. The sample was subsequently cooled to 145 °C and sheared, but without complete recovery of the original hexagonal pattern. (We have shown elsewhere[26] that state B is characterized by a pronounced metastability on cooling and did not make a serious attempt to fully regenerate the HPL state). When the sample was again heated to 210 °C and a relatively high shear rate was applied ($\dot{\gamma} = 2.2\ s^{-1}$), the scattering pattern transformed again. The new pattern contained six relatively strong peaks at approximate angles of $\phi = \pm 20$, ± 160, and $\pm 90°$ and four weaker ones at $\phi = \pm 62$ and $\pm 118°$ (Figure 10d). A comparison of the two 210 °C azimuthal $I(q^*)$ responses is presented in Figure 12. The angular dependence of these ten q^* reflections duplicates the principal SANS peaks obtained when the bicontinuous $Ia\bar{3}d$ phase has been grown from a shear-oriented HEX or HPL state in a variety of other diblock copolymer melts.[26,30,34] The azimuthal relationships between these reflections and the shear direction lend further support for the $Ia\bar{3}d$ space group assignment for state B. Although we do not understand the process leading to these two anisotropic states, the fact that this complement of q^* reflections is obtained suggests a complex response of the bicontinuous $Ia\bar{3}d$ microstructure to dynamic flow fields. These dynamic effects are currently being studied.

4. Discussion

4.1. PI−PS Phase Diagram. Using transition temperatures identified rheologically and ordered state microstructures deduced from TEM and small-angle scattering, we have constructed a "phase diagram" for the PI−PS system. We should note that χN and f are not intensive variables, and so such a depiction is not a proper phase diagram in the strict thermodynamic sense. However, because the phase transition temperatures of these specimens depend sensitively on molecular weight, which may vary over a wide range of values, this parameterization regularizes the results in a way that makes an overall comparison feasible. Our results are illustrated in Figure 13, where we have assumed χ to be independent of composition and taken

$$\chi = 71.4/T - 0.0857 \quad (1)$$

as reported by Rounds,[43] where the segment volume is defined as $v = (v_{PI}v_{PS})^{1/2} \cong 144$ Å^3. This illustration includes the results of all PI−PS samples that we have prepared to date that intercept the ODT at experimentally viable temperatures. The filled circles on the diagram denote order−disorder transitions (ODT's), while the open circles signify the order−order transitions (OOT's). Solid curves have been drawn in this illustration based on the obvious topology dictated by the data points. While we believe that this "phase diagram" is rather comprehensive, we cannot rule out the possibility that additional phases will be identified at intermediate values of f_{PI}. Moreover, the OOT and ODT χN values plotted in Figure 13 may be subject to systematic error due to our assumptions regarding $\chi(T,f)$. Nevertheless, the qualitative features and overall phase topology are not affected by this approximation. The mean-field ODT prediction of Leibler[5] is identified by a broken curve.

Two new nonclassical phases, HPL and bicontinuous $Ia\bar{3}d$, occur on either side of the phase diagram between the LAM and HEX microstructures. These phases are distributed somewhat asymmetrically around $f_{PI} = 0.5$, with the complex phase windows located at $0.36 \lesssim f_{PI} \lesssim 0.39$ and $0.65 \lesssim f_{PI} \lesssim 0.68$. This feature can be attributed to conformational asymmetry, i.e., $\epsilon = \beta_{PI}^2/\beta_{PS}^2 \cong 1.5$,[31] which tends to shift all the OOT curves to f_{PI} values that are larger than what is anticipated for symmetric diblocks. Both weak[5,7,8] and strong segregation[6] theories can account for this effect, which has been observed in other diblock systems we have studied.[31] A particularly clear example of the behavior is provided by the $f_{PI} = 0.24$ and 0.82 specimens, which exhibit only "classical" phases. At $f_{PI} = 0.24$, a small window of BCC spheres separates the hexagonal cylinders and disordered states, while the $f_{PI} = 0.82$ sample contains only hexagonal cylinders as the ordered phase. (We have not confirmed BCC symmetry for the spherical microstructure ourselves. However, this packing has been confirmed by others in various polystyrene−polydiene block copolymers.[44,45]) In the event that the phase behavior were symmetric around $f_{PI} = 0.5$, a larger cubic spheres phase should be found in the latter.

One very obvious aspect of Figure 13 is the absence of the ordered bicontinuous double diamond (OBDD) phase. This bicontinuous cubic microstructure ($Pn\bar{3}m$ space group symmetry) has been widely reported to occur[13,14] in PI−PS diblock and starblock copolymer melts at compositions close to the composition windows where we report the $Ia\bar{3}d$ and HPL morphologies. As recently as 1994, channels of OBDD have been assigned to $0.34 \lesssim f_{PI} \lesssim 0.38$ and $0.67 \lesssim f_{PI} \lesssim 0.72$ in these materials for $\chi N \geq 25$.[16] We believe these OBDD results are incorrect, reflecting two complications that can arise during the preparation and analysis of diblock and starblock samples.

First, unambiguous identification of the $Ia\bar{3}d$ bicontinuous phase by TEM is almost impossible, since

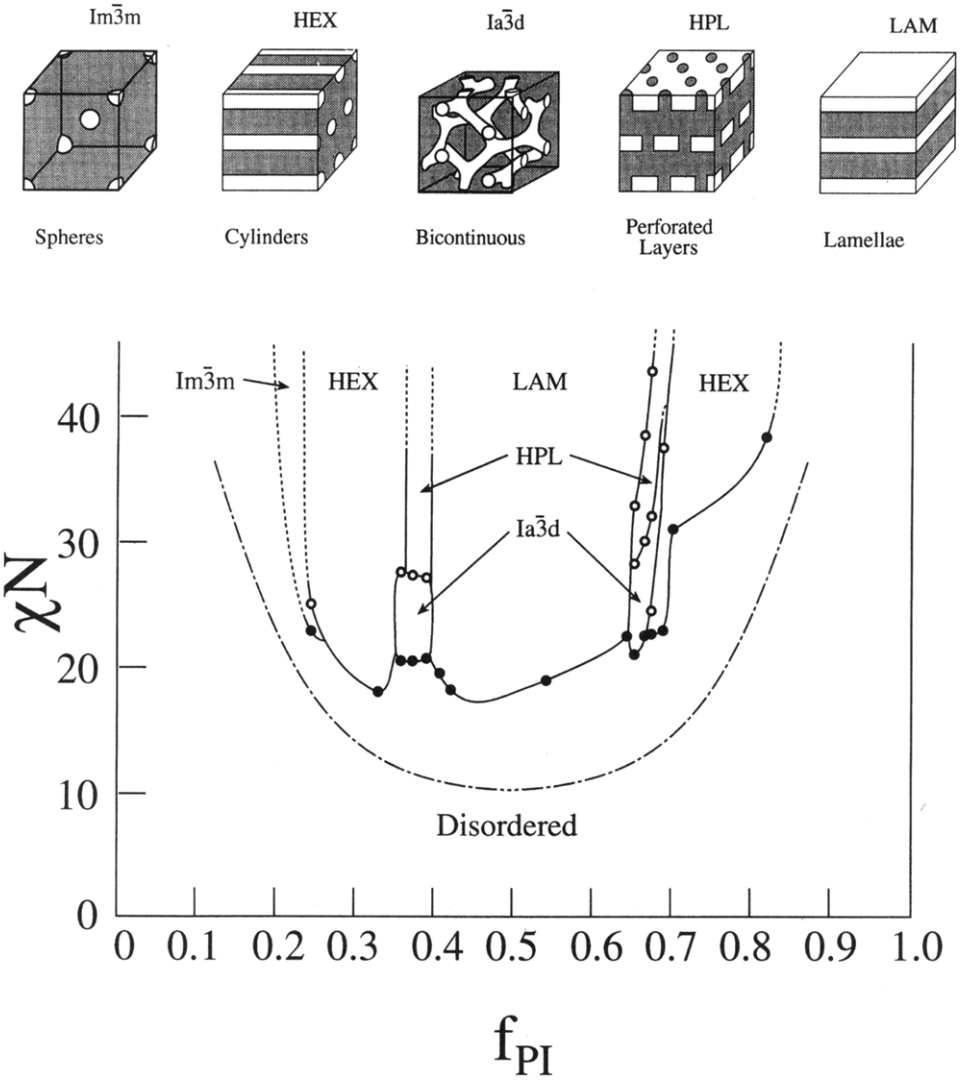

Figure 13. χN versus f_{PI} diagram for PI–PS diblock copolymers. Open and filled circles represent the order–order (OOT) and order–disorder (ODT) transitions, respectively, calculated using eq 1 and the rheologically determined transition temperatures (see Table 1). The dash–dot curve is the mean field prediction[5] for the ODT. Solid curves have been drawn to delineate the different phases observed but might not correspond to precise phase boundaries. Five different ordered microstructures (shown schematically) have been observed by us for this chemical system.

projected images from thin films of this microstructure are nearly indistinguishable from those produced by the OBDD architecture.[27,46] (However, for sufficiently thin films, or large domains, it may be possible to discriminate between the local connector topology, i.e., tripod versus tetrapod.) With few exceptions[13] the OBDD state has been established based on TEM alone. Recently, Hajduk et al.[27] have concluded that an $f_{PI} = 0.67$ PI–PS diblock exhibits a reversible LAM-to-$Ia\bar{3}d$ bicontinuous phase transition based on SAXS as well as TEM analyses. (These authors refer to the bicontinuous $Ia\bar{3}d$ state as the "Gyroid*" phase.) This result is consistent with our phase diagram with one exception: we have not identified a direct lamellae–cubic transition. At least two explanations for this disparity can be advanced: (i) the HPL is a nonequilibrium (metastable) phase, or (ii) the HPL window was missed in the experiments by Hajduk et al.[27] We cannot dismiss either possibility at this time nor resolve this issue with the data at hand. Nevertheless, both studies draw the same conclusion regarding the symmetry of the high-temperature ordered phase. Since then, Hadjuk et al.[46] reexamined several PI–PS (starblock) samples originally associated with the OBDD microstructure[13,47,48] and concluded that the $Pn\bar{3}m$ space group assignment was flawed; SAXS measurements now indicate the $Ia\bar{3}d$ symmetry.

The second complicating factor deals with the profound hysteresis associated with the HEX ↔ $Ia\bar{3}d$ and, to a lesser degree, the HPL ↔ $Ia\bar{3}d$ phase transitions. We have discussed this effect in detail in a previous publication.[26] Here we merely reiterate that the bicontinuous cubic phase can be supercooled far below the apparent equilibrium order–order phase transition. This behavior is most dramatic when dealing with cylinders as the low-temperature phase (see also below). In a separate report that describes experiments conducted with polyethylene–poly(ethylethylene) (PE–PEE) diblocks, we discuss the HEX ↔ $Ia\bar{3}d$ transition and metastability in more detail.[37] Here we suggest that the identification of bicontinuity in the strong segregation limit (SSL) may reflect such metastability due to solvent casting or cooling from elevated temperatures. Recent theory also predicts the absence of either OBDD or $Ia\bar{3}d$ bicontinuous phases in the SSL at equilibrium.[25,49] Note, however, that we cannot rule out the possibility of a metastable OBDD phase, particularly in high molecular weight specimens that would order

in the presence of considerable amounts of solvent. It is just this condition (i.e., excess) solvent that seems to induce OBDD formation in surfactant (lipid)/water systems.[50]

The samples we prepared at $f_{PI} > 0.5$ produced a sequence of phase transitions not observed for $f_{PI} < 0.5$. At $f_{PI} = 0.675$ and 0.692 the bicontinuous phase transforms into hexagonal cylinders before disordering. Because these phase transitions occur at elevated temperatures, we did not attempt a detailed investigation of the association kinetics; degradation is a constant concern above about 150 °C. However, that this transition occurs at all is somewhat surprising given our findings regarding metastability when cooling below the HEX–$Ia\bar{3}d$ boundary. Presumably, the aforementioned hysteresis derives from either a large nucleation barrier or a slow growth rate. Given the epitaxial relationship that dominates the forward reaction, HEX → $Ia\bar{3}d$, we suspect that nucleation presents the greatest limitation to phase transformation. This condition will not be removed by reversing the order of the transition (i.e., $Ia\bar{3}d$ → HEX). Yet, near the ODT cylinders from rapidly from the bicontinuous phase upon heating. Either the kinetics of this transition are highly temperature dependent or a different mechanism facilitates the transition near the ODT. Although we cannot draw any firm conclusions at this point, one enticing possibility is that the $Ia\bar{3}d$ → HEX transition may occur via disordering of the cubic phase following by cylinder formation, which would avoid the epitaxy-dominated kinetics altogether. This implies that near, but below, the ODT the free energies follow the sequence $G_{Ia\bar{3}d} > G_{Dis} > G_{HEX}$. If the $Ia\bar{3}d$ → Dis transition is kinetically favored relative to $Ia\bar{3}d$ → HEX, then the equilibrium transition $Ia\bar{3}d$ → HEX may occur via a transient disordered state, a route that is probably not available when cooling $Ia\bar{3}d$ to HEX (as in ref 26) at lower temperatures. Further heating must bring $G_{HEX} > G_{Dis}$ since an isotropic state results.

The interesting effects induced by shearing the $Ia\bar{3}d$ microstructure (see Figures 10 and 12) suggest that a threshold shear rate exists above which a rotation of the $Ia\bar{3}d$ unit cell about the [111] direction occurs. Based on the predominant principal reflections seen in Figures 10d and 12 (solid curve), we can deduce that the high shear rate places the (110) plane of the cubic unit cell parallel to the shear plane; this can be better visualized using the sketches provided in ref 30. Thus, we seem to obtain the same slip system ({110}⟨111⟩) found in spherically microphase-separated diblock copolymers that contain the $Im\bar{3}m$ space group symmetry[38,51] as well as inorganic BCC crystalline materials.[52]

Finally, we must emphasize that the mechanical properties of ordered block copolymers depend on a variety of factors including microdomain type and orientation, frequency, temperature, mode of deformation (e.g., steady versus oscillatory shear), and relative block entanglement molecular weight. In this paper, we have not attempted to separate these parameters. Rather, we have simply exploited these effects collectively in order to identify phase transition temperatures (Figure 1). This simplistic analysis must be interpreted cautiously. For example, the magnitude and even the sign of changes in $G'(T)$ may depend on the applied frequency and thermal history. Generally, we find that the HEX → $Ia\bar{3}d$ transition is accompanied by a significant increase in G'.[26] However, here we have shown an exception to this trend (Figure 1f) where the isochronal $G'(T)$ trace varies slightly at the HEX → $Ia\bar{3}d$ order–order transition. This may be a consequence of the proximity of this sample to the border of the complex phase window. However, regardless of the origins of this effect, it underscores the need to evaluate in much more detail the relationships between molecular parameters (i.e., N, f, $\chi(T)$), equilibrium microstructure, and dynamical properties.

5. Summary

The χN versus f_{PI} diagram for polyisoprene–polystyrene (PI–PS) diblock copolymers has been characterized near the order–disorder transition. Monodisperse ($M_w/M_n < 1.07$) block copolymers were synthesized and subjected to dynamic mechanical experiments to locate the order–order and order–disorder transition temperatures. Ordered phase symmetries were identified using small-angle scattering (SANS, SAXS) and transmission electron microscopy (TEM). Phase behavior was found to be somewhat complex near the order–disorder transition (ODT). Two nonclassical phases, hexagonally perforated layers (HPL) and a bicontinuous phase with $Ia\bar{3}d$ space group symmetry, were observed at $0.36 \lesssim f_{PI} \lesssim 0.39$ and $0.65 \lesssim f_{PI} \lesssim 0.68$. The bicontinuous phase was found to be stable only near the ODT, while the HPL morphology is found at larger χN values. Experimentally observed $(\chi N)_{ODT}$ values are higher than Leibler's mean-field predictions,[5] suggesting that finite molecular weight effects influence the observed phase behavior.

Acknowledgment. This work was supported by the U.S. Air Force Office of Scientific Research (AF/F49620-93-1-0182) and the Center for Interfacial Engineering (CIE), a NSF Engineering Research Center. I.W.H. and A.J.R. thank the Engineering and Physical Sciences Research Council (U.K.) for support.

References and Notes

(1) Pershan, P. S. *Structure of Liquid Crystal Phases*; World Scientific: Singapore, 1988.
(2) Seddon, J. M. *Biochim. Biophys. Acta* **1990**, *1031*, 1.
(3) Luzzati, V.; Gulik-Krazywicki, T.; Tardieu, A. *Nature* **1968**, *218*, 1031.
(4) Bates, F. S.; Fredrickson, G. H. *Macromolecules* **1994**, *27*, 1065.
(5) Leibler, L. *Macromolecules* **1980**, *13*, 1602.
(6) Helfand, E.; Wasserman, Z. R. In *Developments in Block Copolymers I*; Goodman, I., Ed.; Applied Science: London, 1982.
(7) Fredrickson, G. H.; Helfand, E. *J. Chem. Phys.* **1987**, *87*, 697.
(8) Matsen, M. W.; Schick, M. *Macromolecules* **1994**, *27*, 6761.
(9) Aggarwal, S. L., Ed. *Block Polymers*; Plenum Press: New York, 1970. Molau, G. E., Ed. *Colloidal and Morphological Behavior of Block and Graft Copolymers*; Plenum Press: New York, 1971. Gallot, B. R. M. *Adv. Polym. Sci.* **1978**, *20*, 1651.
(10) Hashimoto, T.; Ijichi, Y.; Fetters, L. J. *J. Chem. Phys.* **1988**, *89*, 2463.
(11) Hashimoto, T.; Yamasaki, K.; Koizumi, S.; Hasegawa, H. *Macromolecules* **1993**, *26*, 2895. Hashimoto, T.; Koizumi, S.; Hasegawa, H. *Macromolecules* **1994**, *27*, 1562. Koizumi, S.; Hasegawa, H.; Hashimoto, T. *Macromolecules* **1994**, *27*, 4371.
(12) Bates, F. S. *Science* **1991**, *251*, 898.
(13) Thomas, E. L.; Alward, D. B.; Kinning, D. J.; Martin, D. C.; Handlin, D. L.; Fetters, L. J. *Macromolecules* **1986**, *19*, 2197.
(14) Hasegawa, H.; Tanaka, H.; Yamasaki, K.; Hashimoto, T. *Macromolecules* **1987**, *20*, 1651.
(15) Kinning, D. J.; Thomas, E. L.; Ottino, J. M. *Macromolecules* **1987**, *20*, 1129.
(16) Winey, K. I.; Gobran, D. A.; Xu, Z.; Fetters, L. J.; Thomas, E. L. *Macromolecules* **1994**, *27*, 2392.
(17) Spontak, R. J.; Smith, S. D.; Ashraf, A. *Macromolecules* **1993**, *26*, 956; *Polym. Commun.* **1993**, *34*, 2233.

(18) Winey, K. I.; Thomas, E. L.; Fetters, L. J. *J. Chem. Phys.* **1991**, *95*, 9367.
(19) Owens, J. N.; Gancarz, I. S.; Koberstein, J. T.; Russell, T. P. *Macromolecules* **1989**, *22*, 3380.
(20) Han, C. D.; Baek, D. M.; Kim, J. K.; Hashimoto, T.; Okamoto, S. *Macromolecules* **1991**, *24*, 5408.
(21) Roe, R.-J.; Fishkis, M.; Chiang, J. C. *Macromolecules* **1981**, *14*, 1091.
(22) Likhtman, A. E.; Semenov, A. N. *Macromolecules* **1994**, *27*, 3103.
(23) Anderson, D. M.; Thomas, E. L. *Macromolecules* **1988**, *21*, 3221.
(24) Hamley, I. W.; Bates, F. S. *J. Chem. Phys.* **1994**, *100*, 6813.
(25) Olmstead, P. D.; Milner, S. *Phys. Rev. Lett.* **1994**, *72*, 936; *Phys. Rev. Lett.* **1995**, *74*, 829.
(26) Förster, S.; Khandpur, A. K.; Zhao, J.; Bates, F. S.; Hamley, I. W.; Ryan, A. J.; Bras, W. *Macromolecules* **1994**, *27*, 6922.
(27) Hajduk, D. A.; Harper, P. E.; Gruner, S. M.; Honeker, C. C.; Kim, G.; Thomas, E. L.; Fetters, L. J. *Macromolecules* **1994**, *27*, 4063.
(28) Almdal, K.; Koppi, K. A.; Bates, F. S.; Mortensen, K. *Macromolecules* **1992**, *25*, 1743.
(29) Hamley, I. W.; Koppi, K. A.; Rosedale, J. H.; Bates, F. S.; Almdal, K.; Mortensen, K. *Macromolecules* **1993**, *26*, 5959.
(30) Schulz, M. F.; Bates, F. S.; Almdal, K.; Mortensen, K. *Phys. Rev. Lett.* **1994**, *73*, 86.
(31) Bates, F. S.; Schulz, M. F.; Khandpur, A. K.; Förster, S.; Rosedale, J. H.; Almdal, K.; Mortensen, K. *Faraday Discuss. Chem. Soc.* **1994**, *98*, 7.
(32) Ndoni, S.; Papadakis, C. M.; Bates, F. S.; Almdal, K. *Rev. Sci. Instrum.* **1995**, *66*, 1090.
(33) Bates, F. S.; Rosedale, J. H.; Bair, H. E.; Russell, T. P. *Macromolecules* **1989**, *22*, 2557.
(34) Krause, S.; Iskandar, M.; Iqbal, M. *Macromolecules* **1982**, *15*, 105; Han, C. D.; Baek, D. M.; Kim, J. K. *Macromolecules* **1995**, *28*, 5886.
(35) Rosedale, J. H.; Bates, F. S. *Macromolecules* **1990**, *23*, 2329.
(36) Winey, K. A.; Patel, S. S.; Larson, R. G.; Watanabe, H. *Macromolecules* **1993**, *26*, 2542.
(37) Zhao, J.; Majumdar, B.; Schulz, M. F.; Bates, F. S.; Almdal, K.; Mortensen, K.; Hajduk, D. A.; Gruner, S. M. *Macromolecules*, to appear.
(38) Koppi, K. A.; Tirrell, M.; Bates, F. S.; Almdal, K.; Mortensen, K. *J. Rheol.* **1994**, *38*, 999.
(39) Bras, W.; Derbyshire, G. E.; Ryan, A. J.; Mant, G. R.; Felton, A.; Lewis, R. A.; Hall, C. J.; Greaves, G. N. *Nucl. Instrum. Meth. Phys. Res.* **1993**, *A326*, 587.
(40) Hamley, I. W.; Gehlsen, M. D.; Khandpur, A. K.; Koppi, K. A.; Rosedale, J. H.; Schulz, M. F.; Bates, F. S.; Almdal, K.; Mortensen, K. *J. Phys. II (Fr.)* **1994**, *4*, 2161.
(41) Disko, M. M.; Liang, K. S.; Behal, S. K.; Roe, R.-J.; Jeon, K. J. *Macromolecules* **1993**, *26*, 2783.
(42) Koppi, K. A.; Tirrell, M.; Bates, F. S.; Almdal, K; Colby, R. H. *J. Phys. II (Fr.)* **1992**, *2*, 1941.
(43) Rounds, N. A., Ph.D. Dissertation, University of Akron, 1970.
(44) Bates, F. S.; Cohen, R. E.; Berney, C. V. *Macromolecules* **1982**, *15*, 589.
(45) Thomas, E. L.; Kinning, D. J.; Alward, D. B.; Henkee, C. S. *Macromolecules* **1987**, *20*, 2934.
(46) Hajduk, D. A.; Harper, P. E.; Gruner, S. M.; Honeker, C. C.; Thomas, E. L.; Fetters, L. J. *Macromolecules* **1995**, *28*, 2570.
(47) Alward, D. B.; Kinning, D. J.; Thomas, E. L.; Fetters, L. J. *Macromolecules* **1986**, *19*, 215.
(48) Kinning, D. J.; Alward, D. B.; Thomas, E. L.; Fetters, L. J.; Handlin, D. L. *Macromolecules* **1986**, *19*, 1288.
(49) Matsen, M. W.; Bates, F. S. *Macromolecules*, submitted.
(50) Turner, D. C.; Wang, Z. G.; Gruner, S. M.; Mannock, D. A.; McElhaney, R. N. *J. Phys. II (Fr.)* **1992**, *2*, 2039.
(51) Almdal, K.; Koppi, K. A.; Bates, F. S. *Macromolecules* **1993**, *26*, 4058.
(52) Barrett, C. R.; Nix, W. D.; Tetelman, A. S. In *The Principles of Engineering Materials*; Prentice-Hall: Englewood Cliffs, NJ, 1973.
(53) Gehlsen, M. D. Ph.D. Thesis, University of Minnesota, 1994.

MA950734+